PERGAMON

Deep-Sea Research I 49 (2002) 915–934

DEEP-SEA RESEARCH
PART I

www.elsevier.com/locate/dsr

Remote-sensing evidence for the local generation of internal soliton packets in the central Bay of Biscay

A.L. New*, J.C.B. Da Silva[1]

James Rennell Division for Ocean Circulation and Climate, Southampton Oceanography Centre, Waterfront Campus, European Way, Southampton SO14 3ZH, UK

Received 17 January 2001; received in revised form 16 November 2001; accepted 4 December 2001

Abstract

Large-amplitude internal solitary waves (or "solitons") occurring in packets near the shelf break in the Bay of Biscay are well-documented and understood. The presence of similar features has now also been reported in the central Bay, $\approx$150 km from the nearest shelf break topography. The present paper analyses available remote-sensing synthetic aperture radar (SAR) data from the ERS satellites in this region. By doing so, we are able to provide convincing support for the hypothesis that these waves, instead of having travelled along the thermocline from the shelf break, are instead generated locally in the central Bay by the surfacing of a beam of internal tidal energy originating from the shelf break. This reinforces the results of a previous independent study, while at the same time providing a much more extensive investigation than was then possible. We have also exploited the large swath width (100 km) and high spatial resolution (100 m $\times$ 100 m) of the SAR to examine for the first time the full surface structure of the internal waves in the central Bay, which are found to have a mean wavelength of 1.35 km, and a mean along-crest "coherence" length of 21.55 km.

Keywords: Internal solitary waves; Synthetic aperture radar; Bay of Biscay (44–48°N, 2–10°W)

1. Introduction

Large internal tidal waves (of semi-diurnal period) are now a well-understood phenomenon in the Bay of Biscay (Fig. 1a). They result from the interaction of the surface tide with the steep shelf-break topography, and those generated by the Celtic shelf slope (47–48°N, 6–8°W) are amongst the most energetic anywhere in the world (Baines, 1982). They are particularly strong near Spring tides, and are manifest, firstly, as long-wavelength oscillations of the seasonal thermocline (typically 35–45 m deep in the summer) which may have vertical crest to trough displacements of 50–60 m near the shelf break. These "thermocline" or "interfacial" internal tides (ITs) travel away from the shelf break both onto the shelf and into the deep ocean, and have been detected with in situ sensors (Pingree and Mardell, 1985; Pingree et al., 1986) and remotely sensed AVHRR "sunglint" imagery in the visible band (Pingree and New, 1995). The shelfward-propagating ITs may travel

*Corresponding author. Tel.: +44-0-2380-596173; fax: +44-0-2380-596204.

E-mail address: a.new@soc.soton.ac.uk (A.L. New).

[1] Present address: Instituto de Oceanografia, Faculdade de Ciências da Universidade de Lisboa, Rua Ernesto de Vasconcelos, Campo Grande, 1700 Lisboa, Portugal.

0967-0637/02/$ - see front matter
PII: S0967-0637(01)00082-6

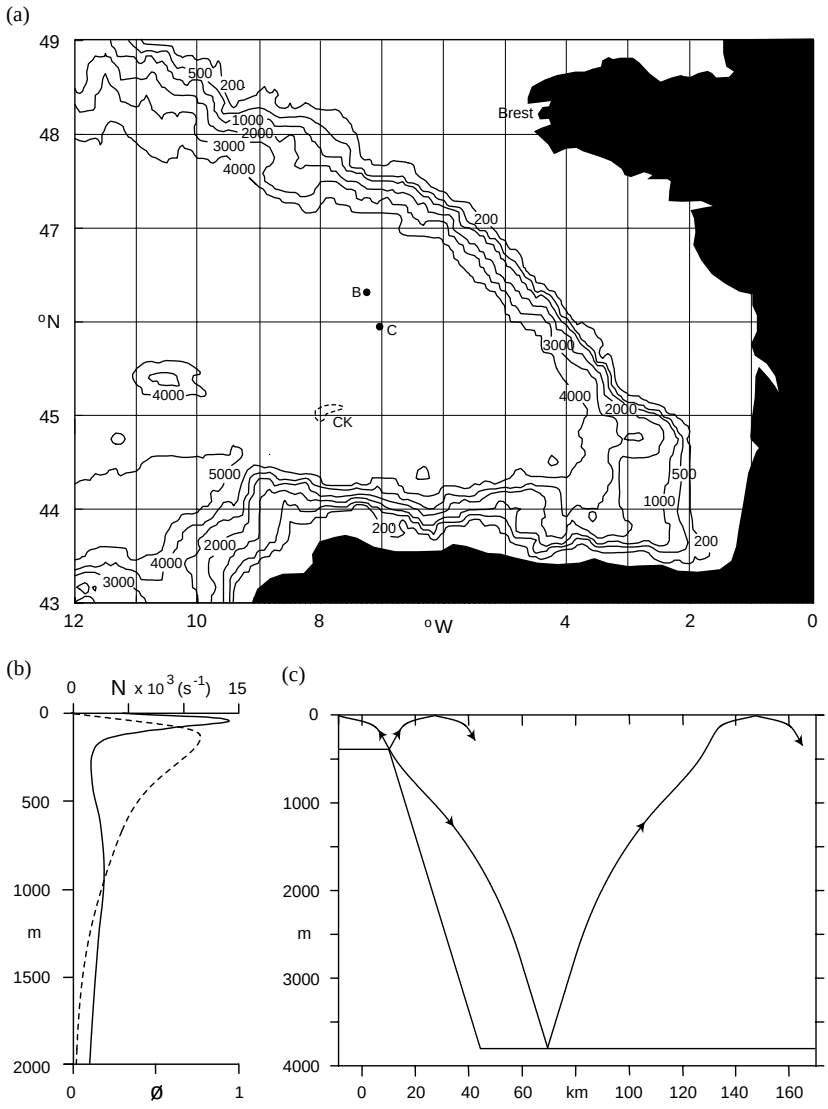

Fig. 1. (a) Chart of the Bay of Biscay, showing depth contours in metres. Cantabria Knoll (CK, near 45°N, 8°W) is indicated by a dashed contour corresponding to 4600 m. Positions B (46°19′N, 7°14′W) and C (45°57′N, 7°02′W) are also shown, as are the coastlines of northern Spain and western France, and the location of Brest. (b) Brunt–Vaisala frequency ($N \times 10^3$, s^{-1}) profile for summer conditions in the Bay of Biscay (solid line), and vertical structure function, ϕ (dashed line, arbitrary scale), for an ISW (see text for details). (c) Characteristic ray paths (for stratification as in (b)) and idealised (model) topography showing the propagation of internal tidal energy away from the shelf break near 47–48°N. Horizontal distance is km into the deep ocean from the 200 m depth contour.

onto the shelf for 200 km or more, and, in the summer, have wavelengths of 30–35 km (and phase speeds of 0.6–0.8 m s^{-1}), while the oceanward tides may travel for over 250 km, and have wavelengths of 45–50 km (and phase speeds of 1.0–1.1 m s^{-1}). They are also typically coherent in the along-crest direction for distances of at least 200 km. The propagation of these thermocline ITs has been successfully modelled by New (1988), Serpette and Mazé (1989), and Gerkema (1996).

The ITs, however, are also evident as "rays" or "beams" of internal tidal energy which follow

characteristic pathways. These rays have a slope c to the horizontal given by

$$c = \pm\left(\frac{\sigma^2 - f^2}{N^2 - \sigma^2}\right)^{1/2}, \quad (1)$$

where N is the local Brunt–Vaisala frequency, σ is the semi-diurnal frequency, and f the Coriolis parameter. A typical summer profile of N in the Bay of Biscay is shown in Fig. 1b (upper 2000 m only for clarity), in which the values of N in the top 600 m are an average from CTDs taken in September 1987 near 6°40′W, 47°25′N (see Pingree and New, 1989), and deeper values are derived from Pingree and Morrison (1973; below 2000 m, these authors show that N continues to decrease exponentially, reaching $0.45 \times 10^{-3}\,s^{-1}$ at 4000 m). The ray-like structure of the ITs in the Bay of Biscay has been modelled, for such a continuous stratification, by New (1988) and Pingree and New (1989, 1991). In this two-dimensional model (cast in terms of distance from the shelf break and depth), three such rays emanate from the "point" of the shelf break (where in nature the topographic slope is equal to c), one ray propagating upwards onto the shelf, and two into the ocean, one upwards and one downwards. This is illustrated in Fig. 1c for a shelf-slope topography appropriate for the Bay of Biscay, and for the Brunt–Vaisala frequencies in Fig. 1b (with $N = 0.92 \times 10^{-3}\,s^{-1}$ below 2780 m providing a suitable approximation to the deeper values). The rays reflect from the sea-surface and sea-floor, and correspond to regions of large-amplitude vertical oscillations which reach up to 400 m (crest to trough) in the deeper ocean. New and Pingree (1990a) showed that these model rays also corresponded to large internal tidal oscillations of the thermocline both near the shelf break (crest to trough amplitudes of order 50 m), arising from the initially upward-propagating rays, and near 150 km into the deep ocean (amplitudes of 90–100 m). This latter position is where the initially downward-propagating ray (which we refer to as the "deep" ray in the following) reaches the surface again after bottom reflection (Fig. 1c). Elsewhere, the modelled tidal displacements of the thermocline were typically only 10–20 m.

In nature, large tidal-period oscillations of the thermocline have indeed been observed both near the shelf break, with typical crest to trough amplitudes of 50–60 m (Pingree and Mardell, 1985; Pingree et al., 1986) and at positions B and C in the central Bay of Biscay (Fig. 1a), with amplitudes of 60–100 m, by New and Pingree (1990a, 1992). The stations B and C lie close to the predicted location of the surface reflection of the deep ray near 150 km from the shelf break. Furthermore, this ray has actually been observed (by making tidal-period CTD stations) to beyond the point of bottom reflection by Pingree and New (1989, 1991), who showed that it had characteristics similar to those of the ray modelled by New (1988). The large internal tidal thermocline amplitudes observed near 150 km from the shelf break then support the view that this ray continues upwards and does indeed reach the surface at about this position, producing these locally large ITs in the thermocline as predicted by the model.

Higher frequency internal waves (IWs) are now also well-documented in the Bay of Biscay near Spring tides. These have also been observed with large amplitudes both near the shelf break (Pingree and Mardell, 1985; Pingree et al., 1986; crest to trough amplitudes of up to 40 m) and at positions B and C in the central Bay (New and Pingree, 1990a, 1992; amplitudes up to 80 m), travelling more or less perpendicularly away from the break. These waves have wavelengths of 1–2 km, periods of 20–40 min, and appear as nonlinear waveforms with steeply penetrating troughs. For this reason, they are usually referred to as internal "solitary" waves (ISWs) or "solitons" in the literature (e.g. Apel et al., 1985). The ISWs typically form packets of between three and eight waves, centred on, or trapped within, the troughs of the thermocline ITs. They almost certainly result from nonlinear and dispersive forces acting on the longer thermocline ITs, much as in the development of an undular bore. This formation process (in which the earth's rotation, f, must be included) has been modelled by New and Esteban (1999) and New and Pingree (2000). They showed that the ISWs would be expected to form quickly, within 6–9 h, from an initial condition representing a long-wavelength internal tide. A similar timescale for the formation

of the solitons at the shelf break is also apparent in the model of Gerkema (1996), who furthermore showed the importance of the earth's rotation in acting to retard this process in the Bay of Biscay.

The ISWs in the internal tidal troughs have been observed to travel at about the same phase speed as the ITs themselves (e.g. $1.1\,m\,s^{-1}$ in the central Bay, New and Pingree, 1990a. This is significantly slower than those observed in the Sulu Sea by Liu et al., 1985, which travel at about $1.9\,m\,s^{-1}$, but this is probably because the thermocline there is both deeper, 130 m, and has larger values of N, up to $20\times10^{-3}\,s^{-1}$). The Biscay ISWs have also been observed to be most likely "mode 1", that is, with vertical oscillations in phase throughout the water column (see Fig. 7 of Pingree and New, 1989). Theoretically, the relative amplitude of the ISW vertical oscillations, given by a vertical structure function ϕ, can be found for a given stratification as in New (1988), assuming the ISWs are small-amplitude (or linear). Using N as in Fig. 1b, a mode 1 ISW of 35 min period was found to travel at only $0.63\,m\,s^{-1}$, i.e. too slowly. However, if the upper 200 m of the N profile was lowered by 35 m to simulate an internal tidal trough, the phase speed increased to $0.91\,m\,s^{-1}$. This seems quite realistic, given that further increases are to be expected due to the nonlinear nature of ISWs. (It also hints that the ISWs can only be trapped in the internal tidal troughs as this is the only place where they can travel quickly enough to keep up with the tides.) The structure function, ϕ, for the ISWs in this latter case is shown in Fig. 1b (dashed line). The vertical oscillations are largest near the thermocline, and decay exponentially with depth.

The large ITs and ISWs at the shelf break and in the central Bay of Biscay are also most probably associated with physical mixing of the water column (Holligan et al., 1985; Pingree et al., 1986; New and Pingree, 1990b, 2000). It therefore seems likely that the energy in the initially upward-propagating internal tidal rays is largely converted into both ISWs and mixing as it passes through the thermocline near the shelf break. This then offers a possible explanation as to why the initially upward- and oceanward-travelling ray has never been observed (e.g. in Pingree and New, 1989, 1991) after its predicted surface reflection (which is why it has not been drawn further into the ocean in Fig. 1c). It therefore seems unlikely that the initially upward-propagating rays play a significant role in the generation of the ISWs in the central Bay.

The large-amplitude thermocline ITs and ISWs in the central Bay are just as large as, if not larger than, those near the shelf break. This led New and Pingree (1990a) to conjecture that the interfacial tides and solitons in the central Bay, instead of having travelled all the way from the shelf break along the thermocline (which would be expected to result in a gradual reduction in their amplitude through dissipation with travel distance), instead had been generated locally in the central Bay by the re-emergence of the deep ray at the surface. Such a resurfacing would, according to the above model studies, be expected to result in large tidal displacements of the thermocline there which would quickly lead to the generation of packets of large ISWs. Indeed, this process has recently been modelled by Gerkema (2001), who showed that the upward-travelling deep ray, when meeting the thermocline, would result in the production of interfacial tides travelling along the thermocline only if the density difference across the thermocline was of an "intermediate" magnitude, of the order of $1.5\,kg\,m^{-3}$. This, however, was noted to be just the case for the summer thermocline in the Bay of Biscay.

This conjecture of "local generation" by New and Pingree (1990a) then led New and Pingree (1992) to undertake five transects with a shipborne acoustic doppler current profiler (ADCP) between the shelf break and 250 km into the central Bay (to near 45°N). The ADCP was able to measure the ISWs, and the study showed that the strongest features indeed occurred both near the shelf break and between 140 and 180 km into the central Bay. The near-shelf ISWs decayed out to about 100 km from the break, and those in the central Bay decayed out to about 250 km. Between 100 and 140 km from the break, no ISWs were detected at all. The authors therefore felt that it was difficult to see how the large ISWs in the central Bay could have travelled all the way from the shelf break along the thermocline, and proposed that this provided strong support for the "local generation"

hypothesis. (A similar mechanism has now also been proposed by Konyaev et al., 1995, to explain large internal waves near the sea surface at about 100 km from a sill on the Mascarene Ridge in the Indian Ocean.)

The main aim of the present paper is to provide a further, independent, examination of the "local generation" hypothesis. This is enabled by an investigation of available synthetic aperture radar (SAR) imagery from remote-sensing satellites. If the wind speed and direction are suitable, this instrument can detect the presence of the soliton packets because of the effect of the ISW surface currents on the roughness of the surface waves, although the modulating effect of surface-active films may also be important (Alpers, 1985; Thompson and Gasparovic, 1986; Ermakov et al., 1992; Da Silva et al., 1998; Brandt et al., 1999; Araújo et al., 2001). Since the swath width of the instrument is 100 km, and its spatial resolution is $100\,\mathrm{m} \times 100\,\mathrm{m}$, we are also able to investigate the horizontal structure of the waves. Section 2 discusses suitable SAR images and provides convincing qualitative support for the hypothesis. A more quantitative analysis is then undertaken in Section 3 which strongly reinforces this conclusion. We here also investigate the wavelengths and along-crest "coherence" lengths of the ISWs.

2. SAR imagery

A search was made of available ERS1/2 SAR archives between 1993 and 2000 for images that revealed the presence of ISWs in the Bay of Biscay. There are, however, several reasons for the relative scarcity of such images. Not only must the wind conditions be suitable for the imaging of the surface effects of the ISWs, but our previous studies have indicated that the internal waves and tides are large only within a few days of a Spring tide: at other times they may be too small to be detected. In addition, the SAR can only be operative for about 10% of its orbit time because of the constraints of power and data storage, and must usually be requested to be switched on. In all, over 40 images were examined, but only four showed clear evidence of ISWs. These were all in mid to late summer, when the thermocline is best developed. This supports the modelling study of Gerkema (2001), which predicts that for a "weak" thermocline (corresponding to the winter case), no ISWs should be generated, whereas for an "intermediate" strength thermocline (corresponding to the summer case), it should be possible to form the ISWs. The four SAR images that revealed ISWs are now discussed.

Our first example, image "A", Figs. 2 and 3, was acquired at 2239 h (GMT) on 14 July 1999. (This is 5.65 h after local High Water at Brest (see Fig. 1a), which occurred at 1700 h GMT. It is also ≈ 1 day after Spring tides at Brest.) Fig. 2 presents the actual SAR image, while Fig. 3 is a representation of this in a Mercator reference frame for ease of interpretation, showing all ISW features of significance. We see firstly a number of overlapping ISW patterns near the shelf break at 47°40′N which to some extent appear to be radiating from "point" sources. (A similar effect was also found by New (1988), where it was concluded that such point sources corresponded to topographic ridges between canyon heads on the upper shelf slope.) There are then some small ISW packets within about 50–60 km southwards of the shelf break, but the next well-defined packet (A_1, see Fig. 3) does not occur until 46°40′N. This comprises three short (in terms of along-crest distances) ISWs which appear (since larger ISWs travel faster and tend to be found on the leading edge of wave packets) to be travelling towards the south-southwest (SSW), in accord with the propagation direction observed in our earlier studies. The next ISW packets towards the SSW are typically much longer-crested and apparently better developed features (packets A_2, A_3 and A_4). The forms of these features are again consistent with propagation to the SSW, and these packets appear to be almost joined together, forming a near-linear feature with an along-crest length of over 90 km. They almost certainly correspond to the same internal tide (IT) depression of the thermocline (remembering that the ISWs always occur in the IT troughs). Consequently, assuming that A_1 corresponds to the next IT trough in towards the shelf break, we estimate the thermocline IT wavelength (from the perpendicular distance

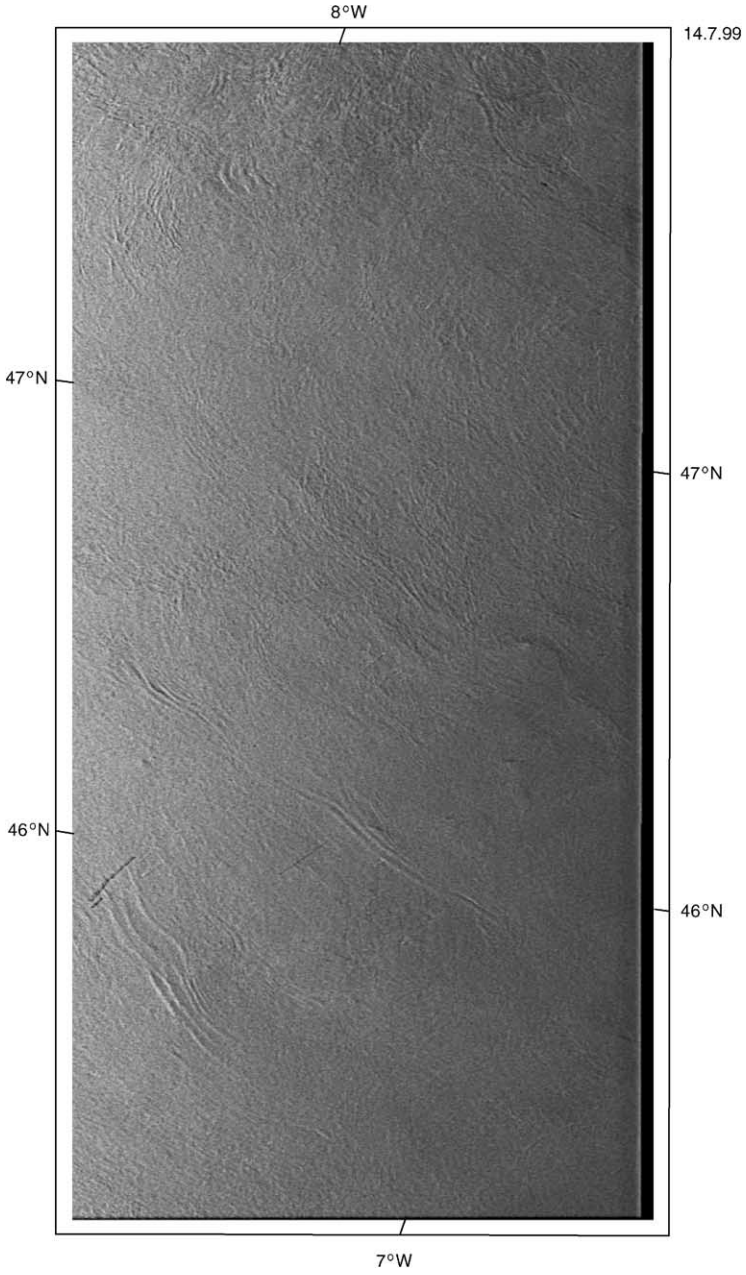

Fig. 2. ERS SAR image "A" in the Bay of Biscay on July 14, 1999 (at 2239 h), extending from the shelf break near 47°30′N into the central Bay. Several ISW packets are visible, the most prominent being near 46°N.

between the mean position of A_1 and a line through the mean positions of A_2, A_3 and A_4) as 48 km. This is in good agreement with Pingree and New's (1995) "sunglint" estimates of IT wavelength at this time of year, between 40 and 45 km. (By "IT wavelength" we specifically mean the wavelength of the interfacial internal tide travelling along the thermocline.) Two other large and

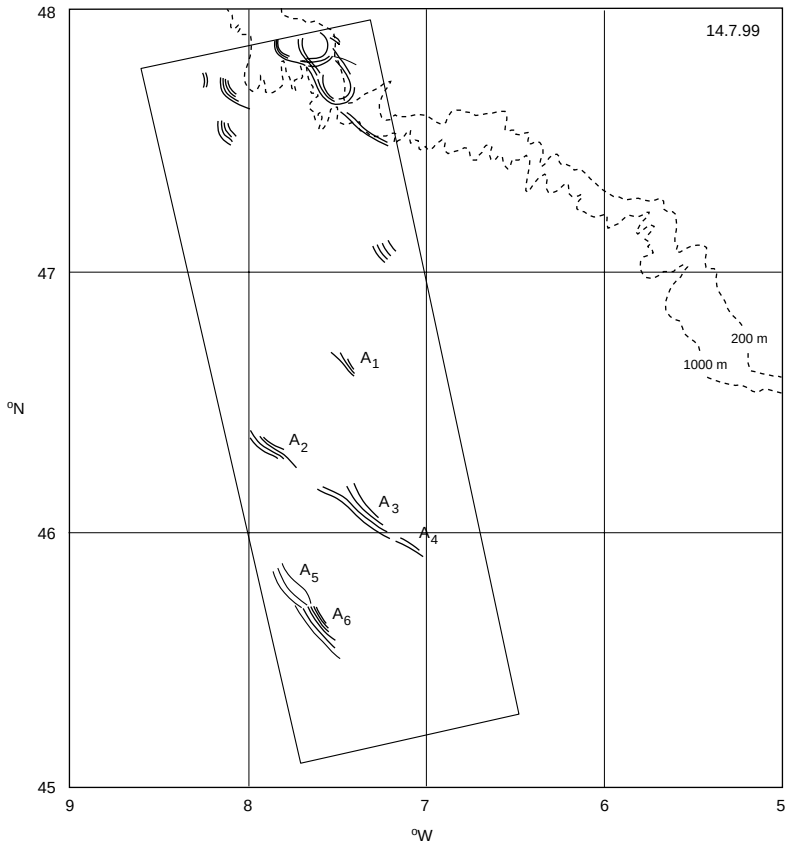

Fig. 3. Interpretation of ERS SAR image A on July 14, 1999 (Fig. 2) in a Mercator reference frame, showing all significant ISW features, and shelf break depth contours (dashed lines). ISW packets in the central Bay are labelled A_1–A_6 (and discussed in the text). Also shown (bold straight lines) is the area covered by the SAR image in Fig. 2.

well-defined ISW packets, A_5 and A_6, are apparent even further to the SSW, and these again appear to be travelling towards the SSW, and seem likely to correspond to the next IT trough away from the shelf break. We calculate (as before) the IT wavelength between these two packets, and A_2, A_3 and A_4, as 47 km, agreeing well with the above estimates.

Overall, image A shows considerable ISW activity near the shelf break, much less between 47°30′N and 46°30′N, and then a local maximum near 46°N, with several well-developed and long-crested wave packets occurring. It therefore provides strong support for the local generation of large ISWs and ITs in the central Bay arising from the surfacing of the deep ray, which would occur between 46°N and 46°30′N. The wavelengths of the ISWs (defined as the distances, perpendicular to the apparent propagation direction, between bright bands in the SAR images), vary between 0.9 and 2.7 km, and the "along-crest" or "coherence" lengths vary between 5 and 37 km. These characteristics, along with the distances of the packets from the shelf break in their apparent direction of propagation, are summarised in Table 1.

We now investigate the other images, and for these, simply show the representations in the geographical reference frame. We also note that the wavelengths and along-crest coherence lengths of the ISWs in these other images fall in approximately the same ranges as for image A

Table 1
Characteristics of the ISW packets in SAR images A, B, C and D further than 60 km from the shelf break (see text for details). Distance from shelf break (km) is measured between the centre of the packet and the 200 m shelf break contour in the apparent direction of travel. The number of waves in each packet, and their ranges of wavelengths (λ km) and along-crest "coherence" lengths (ℓ km) are also given

Packet	Distance from shelf break (km)	Number of waves	Wavelengths (km)	Along-crest lengths (km)
A_1	116	3	1.0–1.4	5–16
A_2	167	4	1.1–1.6	12–24
A_3	183	4	1.6–1.9	17–37
A_4	185	2	1.6	11–14
A_5	238	3	2.1–2.7	22–26
A_6	243	6	0.9–2.3	9–31
B_1	124	5	1.1–2.5	10–19
B_2	128	4	1.2–1.8	19–30
B_3	165	10	0.8–2.0	11–43
B_4	169	3	1.2–2.4	23–34
B_5	174	5	0.7–1.4	12–32
B_6	227	5	0.9–1.8	11–20
B_7	205	5	0.7–1.4	14–27
C_1	61	2	1.6–1.8	18–20
C_2	81	6	0.7–1.1	6–29
C_3	132	5	0.7–1.1	5–17
C_4	186	8	0.7–1.2	6–16
C_5	127	5	1.0	7–19
C_6	144	2	1.0	20–24
D_1	73	4	0.8–1.6	3–36
D_2	96	3	1.0–1.2	19–26
D_3	141	3	1.4–2.0	49–50
D_4	200	4	1.0–1.7	22–38
D_5	241	3	2.2–3.0	32–46
D_6	274	4	1.0–1.6	25–40

(see Table 1 for details), and will not be discussed further until later.

Fig. 4 shows image B, which was acquired at 2236 h on 3rd September 1999. (This is 0.78 h after local High Water at Brest (2149 h) and 5 days after Spring tides here.) It is about 0.75° longitude further to the east than image A. Again, there are numerous ISW packets near the shelf break that appear to be travelling in various directions, giving rise to a complex overall pattern. There are then two packets within 50 km from the break, which were probably generated at the break one tidal cycle before the image was acquired. Further to the SSW, there are then no significant ISW features until about 46°20′N, where two packets (B_1 and B_2) occur. These appear to be moderately well-developed, and, being about the same distance from the shelf break, probably correspond to the same IT depression of the thermocline. The next packets further from the shelf break (B_3, B_4 and B_5) are "stronger" features (waves of greater along-crest lengths, and more waves per packet) and are considered as being fully developed. These packets are also contiguous and are thought of as corresponding to the same IT trough. We estimate the IT wavelength between these packets and (B_1 and B_2) as 42 km, a reasonable value for this time of year. We also note that the best developed of these packets is B_3, which is located close to 46°N, 7°W, where large ITs and ISWs have indeed been directly observed (at positions B and C in Fig. 1a). Further south, there are two more ISW packets, B_6 and B_7. B_6 is propagating in the same general direction as the other packets and is ≈ 59 km further from the break than B_3–B_5. Packet B_7, however, appears to be travelling towards the SSE

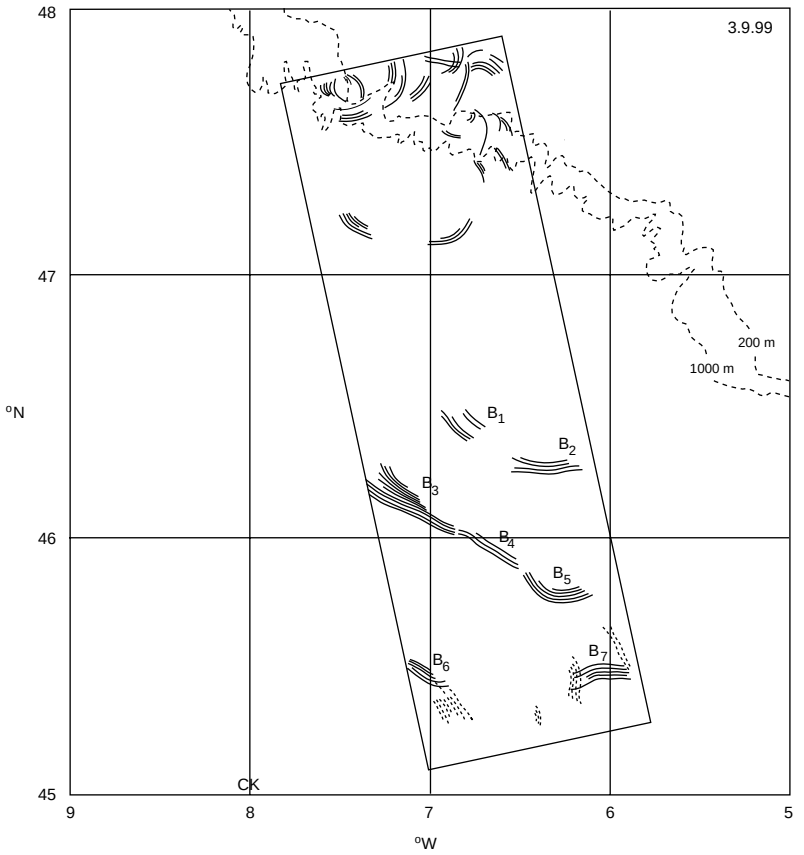

Fig. 4. Interpretation of ERS SAR image B on September 3, 1999 (at 2236 h), showing ISW packets B_1–B_7. Also shown (dashed lines) are wave packets which appear to be travelling towards the ENE between 45° and 45°30′N, possibly arising from the Cantabria Knoll (CK, near 45°N, 8°W). Caption otherwise as for Fig. 3.

and is only 35 km from B_5. It seems possible that these packets represent the next internal tide oceanwards from the shelf break, but that they are being affected by some large-scale advective phenomenon (such as a cyclonic eddy which could be sweeping B_7 northwards, and B_6 southwards). However, these packets are not so well-developed as B_3–B_5, which seems to indicate some dissipation between these locations.

Also apparent in Fig. 4 are further wave packets (dashed lines) near 45°20′N which appear to be travelling towards the ENE. The westernmost of these is about 90 km ENE from Cantabria Knoll, a deep seamount centred at 45°05′N, 8°00′W (CK in Figs. 1a and 4). It therefore seems possible that the packet at 6°55′W could have resulted from the surfacing of an upward-travelling internal tidal ray emanating from the Knoll (e.g. the deep ray in Fig. 1c rises from the sea-floor to the surface in 80 km horizontally). The ISW packet at 6°12′W could then plausibly be the wave packet generated from the Knoll on the previous tide.

Image C, Fig. 5, was acquired at 2233 h on 15th August 1999. (This is 3.92 h after local High Water at Brest (1838 h) and 3 days after Spring tides.) It is about 0.75° longitude further east than image B. Again, we see a complex variety of wave packets near the shelf break, and two more just oceanwards of the break which were probably generated on the previous tidal cycle. Further southwards, the next packets, C_1 and C_2, are separated by only 14 km. This is too short for an IT wavelength, so their generation mechanism is not clear, unless they too are being affected by some large-scale

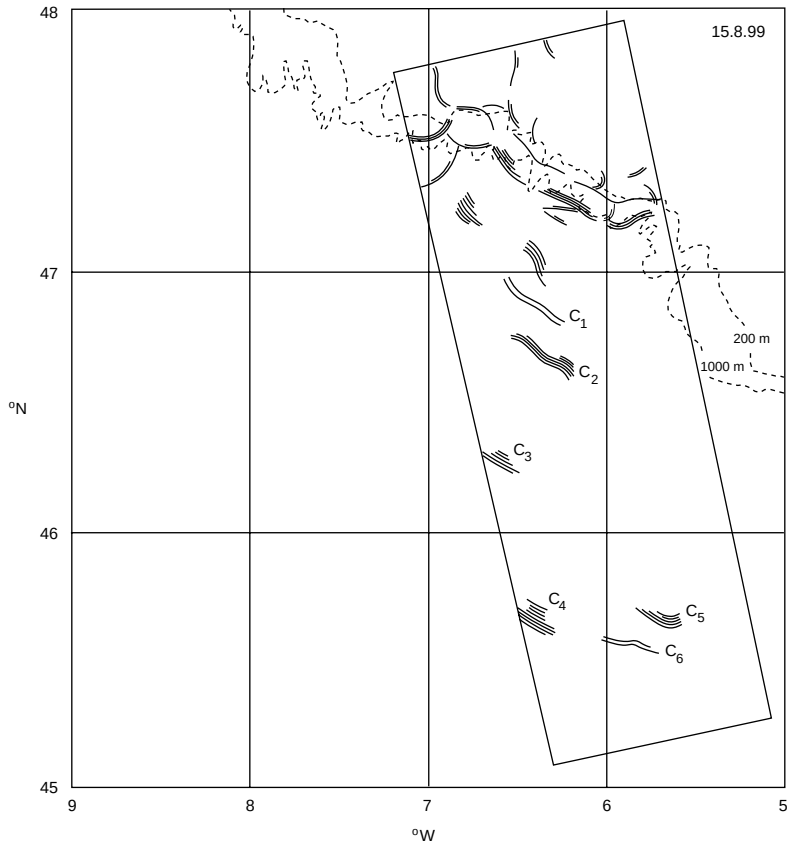

Fig. 5. Interpretation of ERS SAR image C on August 15, 1999 (at 2233 h), showing ISW packets C_1–C_6. Caption otherwise as for Fig. 3.

advective phenomenon (such as a mean current towards the shelf break). However, the next two packets out from the break, C_3 and C_4, are separated by approximately IT wavelengths from each other and from C_2. For instance, C_3 is 47 km from C_2, and C_4 is 48 km C_3. Two further packets, also travelling generally southwards, occur near 45°40′N (C_5) and 45°35′N (C_6), but are not separated by IT wavelengths. However, it seems possible that C_6 could form part of the same internal tidal trough as C_4, and that C_5 could form part of the same trough as C_3, though generated by a different part of the shelf break (e.g. that near 5°15′W). There could also be some advective feature or eddy as before, acting to sweep C_5 and C_6 together. (Note that this image is only 19 days before image B, so that the same eddy could be present in both near this location.) This image does not provide such positive support, as compared with A and B, for larger ISWs in the central Bay than elsewhere, but this could be because it is significantly further east, and does not cover the region near 46°N, 7°W where large ISWs occur in images A and B and have been observed in situ.

Our last example, image D, Fig. 6, was acquired at 1117 h on 22nd July 1994. (This is 7.97 h after local High Water at Brest (0319 h) and 2 days before a Spring tide.) As in images A and B, there are multiple wave packets radiating from sources near the shelf break, two packets further off shelf (D_1 and D_2) which are not particularly well-developed, and a series of further packets (D_3–D_6) in the central Bay which are more well-developed. This again supports the local generation hypothesis. Whilst D_1 and D_2 are quite close together

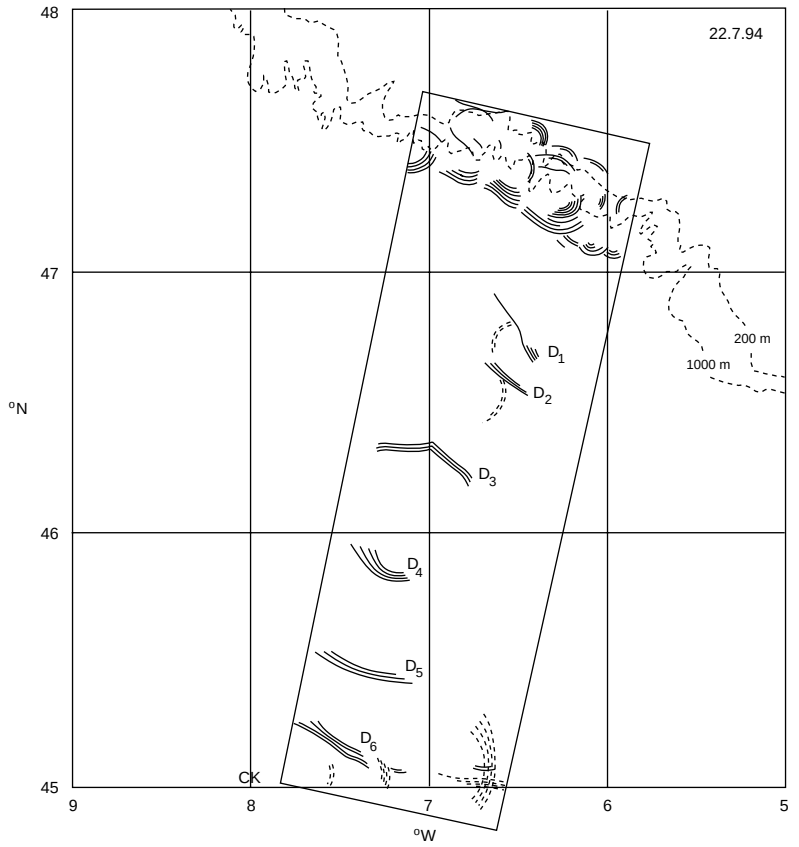

Fig. 6. Interpretation of the ERS SAR image D on July 22, 1994 (at 1117 h), showing ISW packets D_1–D_6. Also shown (dashed lines) are wave packets which appear to be travelling towards the *E* near 45°N, possibly arising from CK, as well as some other unexplained wave packets (see text). Caption otherwise as for Fig. 3.

(17 km, implying that they are either generated by the same tidal cycle but different parts of the shelf break, or that they are being affected by an advective process), the other wave packets are separated by distances which correspond approximately with internal tidal wavelengths (there being 44 km between the eastern portion of D_3 and D_2, 53 km between D_4 and D_3, 43 km between D_5 and D_4, and 32 km between D_6 and D_5). The differences in these IT wavelengths could result either from the presence of eddies (or other large-scale current structures), or from horizontal differences in density structure which would affect the propagation speed of the ITs. We note the presence of two packets (dashed lines) between D_1 and D_2, and just south of D_2, the origins of which are unknown (unless the latter is generated by the Trevelyan Escarpment near 46°45′N, 8°30′W), and the presence of further wave packets (dashed lines) near 45°N which seem to result from the Cantabria Knoll as in image B. There is also a wave packet near 45°N which appears to be travelling northwards and could have been generated by the Spanish shelf break. We finally note that D_3 comprises waves travelling in two different directions, which could indicate two packets from different regions of the shelf break, or that refraction of the wave crests has occurred on encountering a sharp horizontal change in the density structure.

Fig. 7 now shows a composite from images A, B, C and D of all packets either near the shelf break or travelling approximately towards the S or SSW. Also shown are copies of the 200 m shelf

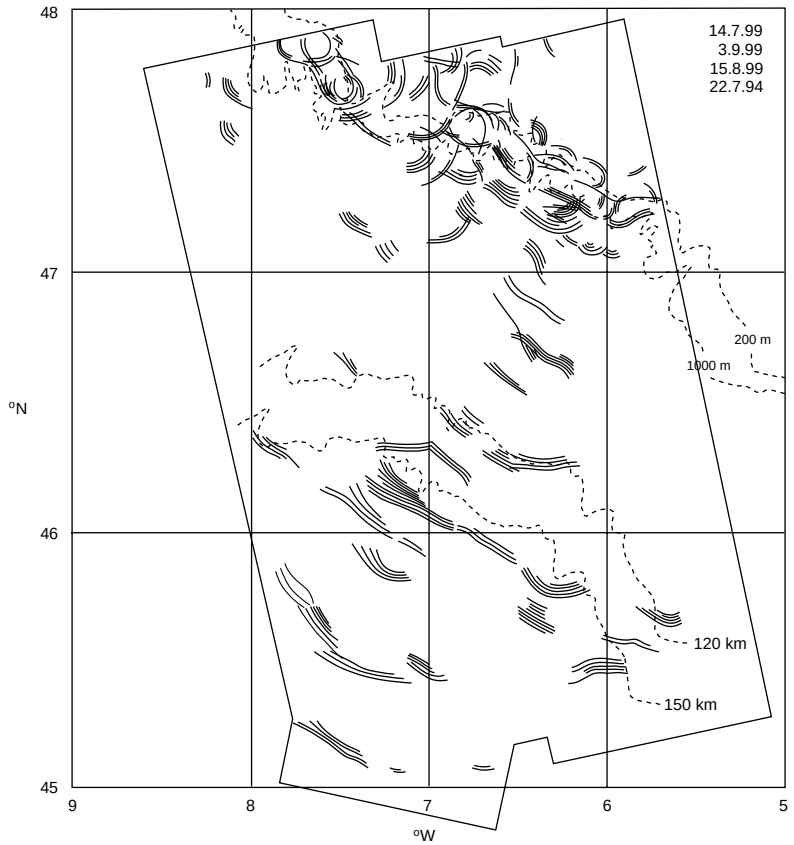

Fig. 7. Composite of all ISW packets observed in SAR images A, B, C and D which are either close to the shelf break between 47° and 48°N, or are travelling approximately directly away from this zone. (This excludes only those wave packets shown as dashed lines in images A, B, C and D.) In addition to the shelf break depth contours, copies of the 200 m contour displaced towards the SSW by 120 and 150 km are also shown (bold dashed lines). The envelope of the areas covered by the SAR images is indicated by the bold straight lines.

break contour displaced by 120 and 150 km towards the SSW (and labelled accordingly). We clearly see the complex pattern of numerous energetic ISW packets generated directly at the shelf break. These extend for about 60 km from the break, though in decreasing numbers. Then between 60 and 120 km from the break, far fewer ISWs are observed. However, at larger distances to the SSW, the level of ISW activity increases markedly. This seems to reach a maximum between about 150 and 180 km from the break, before declining with further distance to the SSW. The location of this maximum is entirely consistent with our expectations, given that the internal tidal ray may typically cover several hundred metres in vertical extent (Pingree and New, 1991). For instance, we might expect the first appearance of "small", developing ISWs about 120 km from the break, where the ray might first start to affect the thermocline (Fig. 1c), and that "large", well-developed ISWs would not occur until somewhere beyond the surface reflection of the deep ray. For instance, in Fig. 1c the deep ray first passes through the thermocline near 130–140 km from the shelf break. If this initiates large thermocline ITs travelling away from the break, and we anticipate about 0.5–0.75 of a tidal cycle elapsing before the ISWs become fully developed (see above), then fully developed ISWs would first be expected about 150–180 km from the break, in

excellent agreement with Fig. 7. Fig. 7 therefore provides strong support for the "local generation" hypothesis that the increased ISW activity in the central Bay is due to the surfacing of an internal tidal ray.

3. Quantitative analysis

We now provide a more quantitative analysis of the ISWs, and Fig. 8 shows the total number of ISW packets (N_1), the total number of ISWs (N_2),

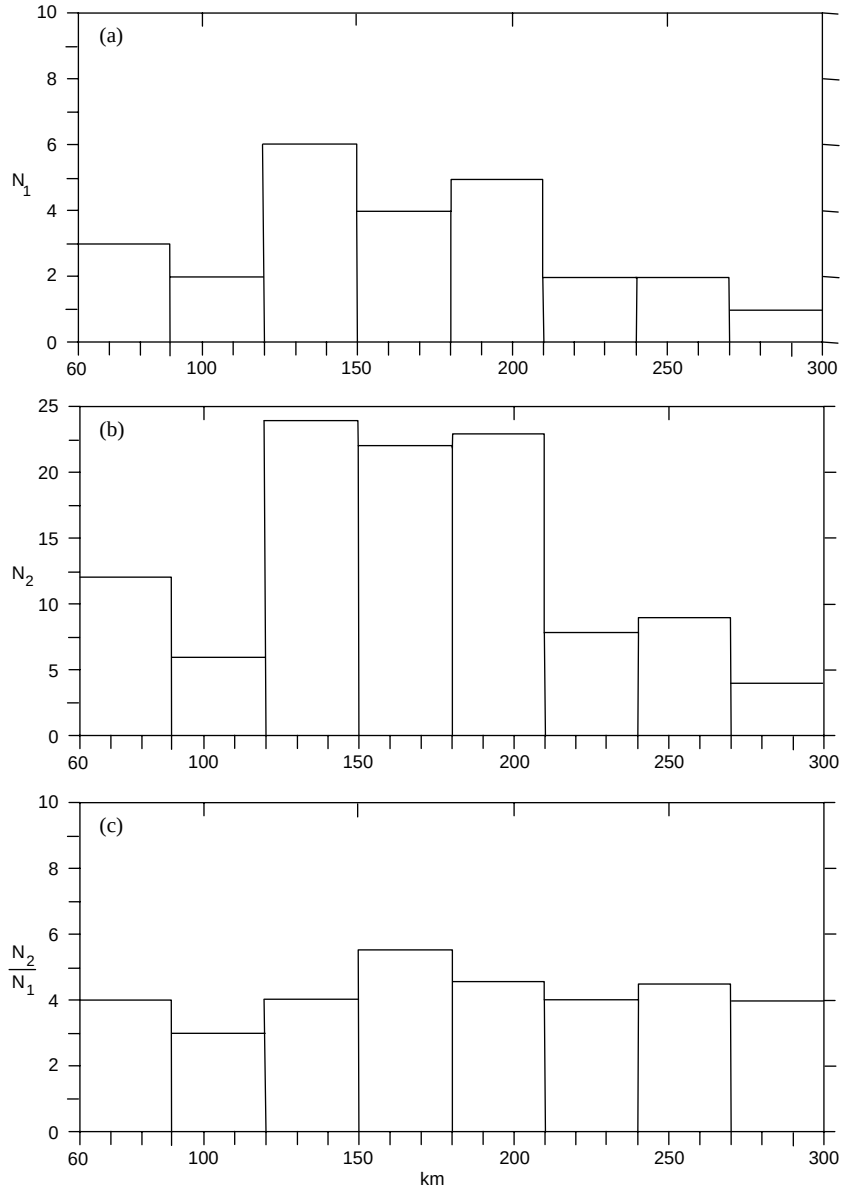

Fig. 8. Frequency of occurrence of ISWs travelling away from the shelf break, and accumulated over all labelled wave packets in images A, B, C and D. These are plotted against distance from the 200 m shelf break contour in bands 30 km wide (commencing at 60 km from the shelf break). (a) N_1, total number of ISW packets in each band. (b) N_2, total number of individual waves in each band. (c) Average number of waves per packet (N_2/N_1).

and the average number of waves per packet (N_2/N_1), in bands of width 30 km extending oceanwards from the shelf break. Here we have taken the distance of each wave packet from the 200 m shelf break contour in its apparent direction of propagation (see Table 1), and have not included waves closer than 60 km to the shelf break (because of the complexity of the patterns there), resulting in a survey comprising the 25 wave packets previously discussed (A_1–A_6, B_1–B_7, C_1–C_6 and D_1–D_6). Fig. 8a shows that the number of ISW packets in each 30 km band (clearly large near the shelf break) drops with distance from the break out to 90–120 km, but then is much higher between 120 and 210 km, before decreasing again out to 270–300 km. The total number of ISWs in each band follows a similar pattern (Fig. 8b), with values falling to a minimum between 90 and 120 km, rising dramatically between 120 and 210 km, and then falling again with further distance from the shelf break. We also consider the average number of ISWs per packet, since we would expect this number to become larger as the packets evolve to become fully developed, and then to decrease again with further travel distance as the ISWs become affected by various dissipation mechanisms. Fig. 8c shows that these numbers fall out to 90–120 km from the break, but then again increase to a maximum between 150 and 180 km, before again generally decreasing out to 270–300 km. All these indicators show that the levels of ISW activity do indeed reach a local maximum in the central Bay of Biscay (centred between 150 and 180 km), providing further support for the "local generation" hypothesis.

We now assess a proxy for the "strength", and other parameters, of the ISWs by analysing profiles of backscattered SAR intensity in the wave packets. An example is shown in Fig. 9. This is a profile taken perpendicularly to the wave crests through the centre of packet B_3, and shows only the five ISWs nearest the back (NNE) of the packet (for clarity), with distance being measured to the NNE. The quantity plotted is a normalised backscatter intensity given by

$$K = (I - I_0)/I_0, \tag{2}$$

where I is the direct backscattered intensity, and I_0 is a "background" value taken to give K a zero mean for the waves in question. (Usually, this is an average over a small area, typically 3–4 km square, near to, but undisturbed by, the ISW packet.) This enables us to investigate the wave-induced variations relative to the background state. It also removes the algebraic dependence of the SAR return on the slant range (which produces the general bright to dark contrast from left to right in Fig. 2). This means that we can then sensibly

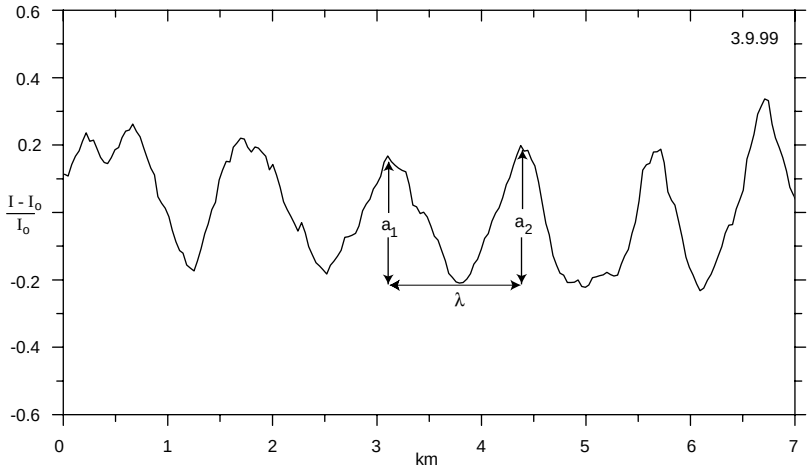

Fig. 9. Example of normalised SAR backscatter return ($(I-I_0)/I_0$) through packet B_3 on September 3 1999, plotted against distance (km) to the NNE. Also shown are the parameters a_1, a_2 and λ required for the calculation of E. (See text for further details.)

compare properties from wave packets at different ranges. We retrieve the (crest to trough) "amplitude" and wavelength of the waves as determined from their profiles of K. For waves that appear as dark bands in the SAR images, or as alternating dark and bright bands (as is the case in Fig. 9), the amplitude of any particular wave is taken as the mean of the difference in K from the preceding crest to the trough in question, and from that trough to the following crest (i.e. as $a = (a_1 + a_2)/2$ where a_1 and a_2 are as shown in Fig. 9). The wavelength is then taken as the distance from the preceding crest to the following crest (see λ in Fig. 9). For waves that appear as bright bands, suitably corresponding definitions are taken.

By analogy with surface waves, we now define a total "energy proxy" in a packet of ISWs as

$$E = \sum_{i=1}^{N} a_i^2 \lambda_i \ell_i, \tag{3}$$

where there are N waves, with index i, in the packet, and the ith wave has amplitude a_i, wavelength λ_i, and along-crest "coherence" length ℓ_i. For each wave, a_i, and λ_i are taken as the mean values over multiple (usually 2 or 3 per packet) profiles of K, and $\ell_i$is measured directly from the SAR images. The quantity E does not represent the physical energy in the waves, but serves as a proxy measure of their "strength". As before, we include only waves in the 25 wave packets A_1–A_6, B_1–B_7, C_1–C_6 and D_1–D_6, giving a survey over 108 waves in total, and the ranges of λ_i and ℓ_i for each wave packet are given in Table 1.

Fig. 10 shows the distributions of λ_i and ℓ_i. The wavelengths (Fig. 10a) fall between 0.6 and 3 km, with the majority (80%) between 0.8 and 2.0 km. The distribution is skewed towards the lower values, with the largest numbers falling between 0.8 and 1.4 km, and progressively fewer at higher wavelengths. The mean value is 1.35 km. These results are consistent with previous in situ estimates derived from observations on the ship's radar by New and Esteban (1999). Fig. 10b shows the distribution of the along-crest "coherence" lengths. These range from a few km up to 50 km. Their distribution is slightly skewed towards the lower values, but not so much as for the wavelengths. The highest frequencies of occurrence are between 10 and 25 km, and the mean value of all the waves observed is 21.55 km.

Fig. 11a now presents the distribution of the ISW energy proxies (E) in terms of distance from the shelf break. We have summed the contributions from all packets into bands of width 30 km, as before. The combined energy proxies of the packets close to the shelf break will clearly be high. Even between 60 and 90 km, the total value of E is still large (nearly 130), being the highest band average in the survey. However, between 90 and 120 km, the value of E has fallen to its lowest level, about 10. The values then start to increase with further distance from the break, reaching over 50 between 120 and 150 km from the break, and achieving a local maximum of 110 between 150 and 180 km. At still larger distances, the levels then generally decrease out to 270–300 km.

However, the amplitude of the SAR backscatter returned from a given packet of ISWs depends on the wind speed and direction, as already discussed (Brandt et al., 1999; Araújo et al., 2001). There could therefore be some bias in the distribution of E in Fig. 11a towards those images for which the wind conditions were particularly favourable for the production of large-amplitude backscatter returns. We have investigated this by evaluating the mean ISW packet E-values for each image. These were found to be 16.25, 20.27, 22.47 and 11.38 for images A, B, C and D, respectively. We see that the distribution of E in Fig. 11a would therefore somewhat over-emphasise images B and C, while under-representing images A and D. We may remove this bias by rescaling the E-values for each packet so that the mean E-value for each image is identical. This leads us to the definition of E^*, the "rescaled energy proxy", which is such that its mean value for each image is 20.0. (Thus, for instance, the ISW packet E-values in image A were all rescaled by 20.0/16.25, and similarly for the other images.) The resulting distribution of E^* in Fig. 11b is remarkably similar to the distribution of E, which indicates the robustness of our result. Again, band-averaged values of E^* fall from high values near the shelf break to a clear minimum between 90 and 120 km, and then rise steadily to a pronounced local maximum in the central Bay

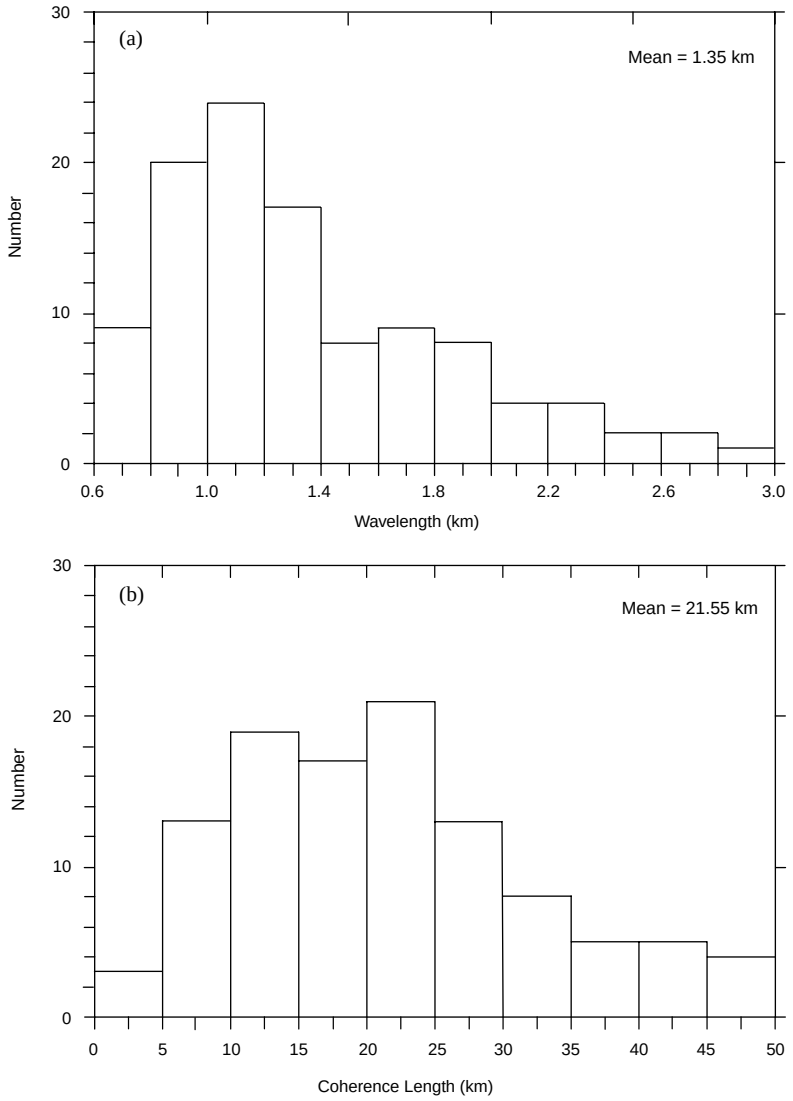

Fig. 10. Distributions of ISW parameters in the central Bay of Biscay (further than 60 km from the shelf break) accumulated over all labelled wave packets in images A, B, C and D. (a) Wavelength (km). (b) Coherence length or along-crest length (km).

between 150 and 180 km, before generally decreasing out to 270–300 km. Overall, we therefore take the distributions of E and E^* as strongly supporting the local generation hypothesis.

4. Summary and discussion

The main goal of the present paper has been to examine the "local generation" hypothesis that large-amplitude ISWs are generated locally in the central Bay of Biscay by the surfacing of a ray of internal tidal energy. This has been achieved by an investigation of four ERS SAR images, comprising 25 ISW packets and 108 individual waves. The images are at $\approx$1, 4, 6 and 8 h after local High Water at Brest, so that our analysis is not biased to any particular state of the surface tide. The ISW packets in the central Bay typically occurred with a spacing corresponding to a thermocline internal

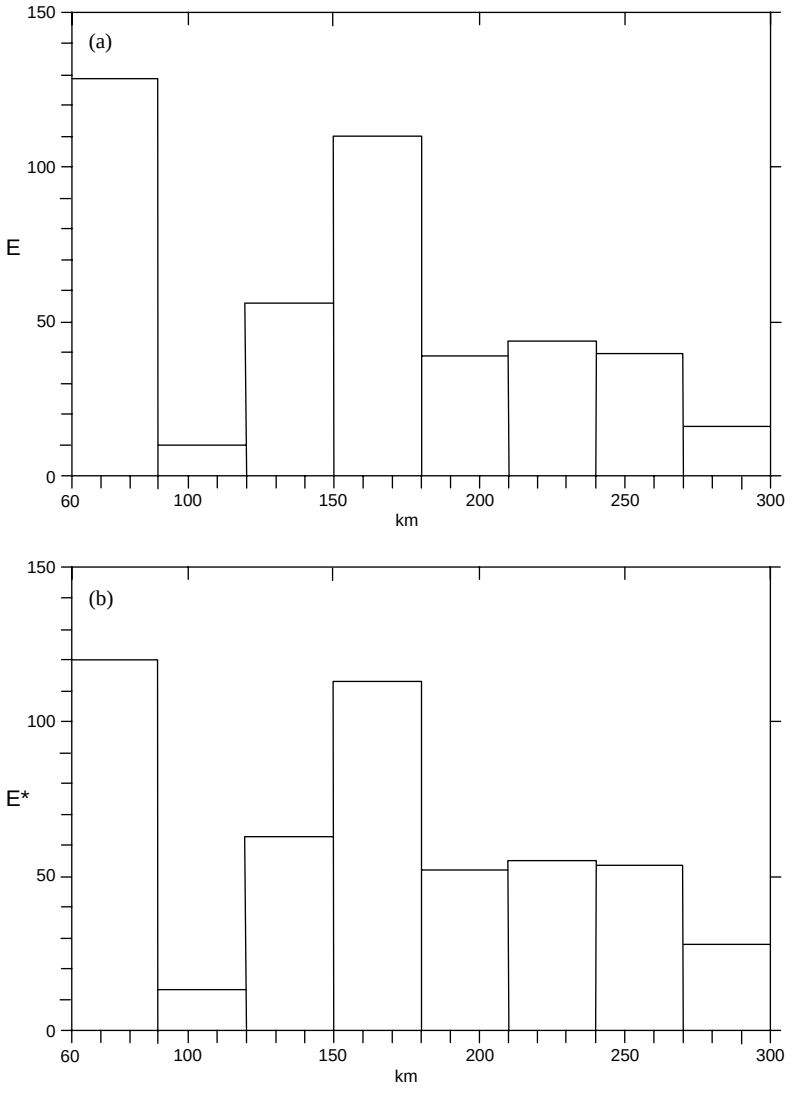

Fig. 11

Fig. 11. (a) Distribution of ISW packet "energy proxy", E, accumulated over all labelled wave packets, and plotted against distance from the shelf break (200 m contour) in bands 30 km wide. (b) As for part (a), except now showing the "rescaled energy proxy", E^*.

tidal wavelength, and larger numbers of ISWs were indeed found in the central Bay as compared with neighbouring areas. The levels of ISW activity were investigated quantitatively, with a range of indicators showing an initial general decrease away from the shelf break (reaching a minimum between 90 and 120 km from the break), but then rising levels in the central Bay, with a maximum centred between 150 and 180 km from the break, and finally, decreasing activity with further distance oceanwards (to 300 km from the break). This behaviour was found to be completely in accord with, and hence strongly supports, the local generation hypothesis, in which the deep

internal tidal ray would pass through the thermocline near 120–150 km offshelf, generating ISWs in the central Bay which would be expected to become fully developed between 150 and 180 km offshelf.

We therefore believe that ISWs are generated both at the shelf break, and in the central Bay, and that this gives rise to the bi-modal distributions seen in Figs. 7 and 11, for instance. The present study shows that both sets of ISWs decay over about 90–120 km of travel. Such dissipation presumably occurs through mechanisms such as mixing, radial spreading, viscous dissipation, and, possibly, wave–wave interactions. This result confirms the conclusions of New and Pingree (1992), who, using a shipborne ADCP, found a remarkably similar bi-modal distribution of ISW activity. However, the present investigation has allowed a more intensive survey than that of New and Pingree (1992), comprising the study of 108 ISWs rather than 38, so giving a correspondingly greater level of confidence in the results.

The use of the ERS SAR, with a swath width of 100 km and a spatial resolution of 100 m × 100 m, has also enabled us to study the full two-dimensional structure of the ISWs for the first time. As a secondary goal, we have therefore examined the distributions of the ISW wavelengths and along-crest "coherence" lengths. We have shown that the ISWs have a mean wavelength of 1.35 km. This compares well with a previous in situ estimate of about 1.6 km inferred by New and Esteban (1999) from seven ISW packets observed on the ship's radar near position C (Fig. 1a). However, with the much larger sample size, we have here been able to refine this estimate. We have also shown that the mean value of the coherence lengths of the ISWs is 21.55 km, and believe that this is the first time that such an estimate has been made (our previous studies with the ship's radar only revealing typically 6–8 km of their along-crest structure). This illustrates the usefulness of the SAR. (We note, however, that some of the ISW packets were only partially visible within the SAR viewing region, so that the present distribution of coherence lengths is likely to be biased slightly towards the low side.)

This study has shown that the large proportion of ISWs in the Bay of Biscay appear to be generated (either directly, or indirectly due to the surfacing of the deep ray) by the shelf break between ≈5°40′W and 6°40′W, and to propagate towards the SSW, directly away from the shelf break (Fig. 7). Indeed, Baines (1982) applied an internal tidal generation model to various areas of the world's shelf breaks, and concluded that the Biscay shelf between 47 and 49°N (i.e. 5°30′–11°00′W) supported the largest internal tidal energy flux of all those regions studied. Serpette and Mazé (1989), in a more detailed study of only the Bay of Biscay, used a two-layer model to show that the shelf break between 5°40′W and 7°10′W was responsible for the generation of the largest ITs, due to a combination of the strongest barotropic forcing and steep topography. The area of our present study therefore provides an ideal testbed for an investigation of the ITs and resulting ISWs.

We now remark that (e.g. in Fig. 7) the highest levels of ISW activity in the central Bay seem to occur near 46°N, 7°W. This is probably because this area is both directly "downstream" from the major generation site on the break between 5°40′W and 6°40′W, and also near to where the internal tidal ray should surface. An alternative explanation of the high levels of ISW activity in the central Bay could also derive from the fact that the shelf break between 5° and 7°30′W takes the form of a near-circular arc with a centre close to 46°N, 7°W, and that this could act to "focus" interfacial ITs, travelling along the thermocline, in the central Bay. However, Serpette and Mazé (1989) show no evidence for such locally large thermocline ITs resulting from focusing. On the contrary, the amplitudes of their interfacial tides decline quickly as they approach 46°N, 7°W. We therefore believe that the surfacing of the deep ray (an effect which is not captured by the two layer model of Serpette and Mazé, 1989) offers a more likely explanation for the presence of the ISW packets in the central Bay. (Perhaps, though, such rays, generated by different points along the "circular-arc" shelf break, could plausibly be subject to some such focusing phenomenon.)

We further remark that we have also detected some evidence for the generation of ISW packets, travelling towards the ENE, by Cantabria Knoll. This is a deep seamount (situated near 45°N, 8°W) with a summit about 4300 m below the surface. However, although a tidal ray emanating from its sides could surface near to the position at which these ISW packets are first observed, further study is needed to verify this mechanism.

Finally, we contrast the situation in the Bay of Biscay with that in the Sulu Sea, as revealed by Liu et al. (1985). In the Sulu Sea, the ISWs radiate from a point source (a topographic saddle point), but are not visible in satellite imagery until they are about 190 km (two internal tidal wavelengths) downstream from the source. The propagation of these ISWs was modelled, assuming they travelled along the thermocline, and the effects of radial spreading and dissipation were shown to be significant. In particular, the model revealed rapid growth of the ISWs in the region just before they were observable in the satellite imagery, followed by gradual decay further downstream. The Biscay situation is different in that plentiful ISWs *are* observed near their (shelf-break) source, and that these decay to low levels between 90 and 120 km from the break, before again increasing further out. It is therefore difficult to see how this "maximum–minimum–maximum" situation could be explained by the Sulu Sea scenario, in which only one "maximum" is observed. We further remark that whereas thermocline ISW amplitudes of 40 m or more may be needed before the waves are satellite-visible in the Sulu Sea, a "detection threshold" somewhere in the range 15–20 m may be more appropriate for the Bay of Biscay (i.e. see Fig. 3 of Pingree et al., 1986), but this may be due to the Biscay thermocline being much shallower (40–50 m) than that in the Sulu Sea (120–130 m).

In conclusion, it does not seem credible that the high levels of ISWs that occur in the central Bay of Biscay, in conjunction with the lower levels closer into the shelf break and the higher levels actually at the shelf break, could have resulted from the propagation of the ISWs along the thermocline all the way from the shelf-slope region. (If this were the case, we would expect gradually decreasing levels of activity with increased distance from the "maximum" at the shelf break, and not a "maximum–minimum–maximum" as observed.) The present paper therefore provides convincing support for the local generation of ISW packets in the central Bay of Biscay due to the surfacing of the deep internal tidal ray from the shelf break.

Acknowledgements

The ERS SAR image data presented here was provided by the European Space Agency (ESA) under project number AO3–177, and J.da S. was supported by Programa PRAXIS XXI BPD/14165/97. We also thank Theo Gerkema, and anonymous reviewers, for providing helpful comments on early versions of the paper, and Robin Pingree for several stimulating discussions on the subject of internal waves.

References

Alpers, W., 1985. Theory of radar imaging of internal waves. Nature 314, 245–247.

Apel, J.R., Holbrook, J.R., Liu, A.K., Tsai, J.J., 1985. The Sulu Sea internal soliton experiment. Journal of Physical Oceanography 15, 1625–1651.

Araújo, I.B., Da Silva, J.C.B., Ermakov, S.A., Robinson, I.S., 2001. On the role of wind direction in ERS SAR signatures of internal waves on the Iberian Shelf. Accepted in The Global Atmosphere and Ocean System, October, 2001.

Baines, P.G., 1982. On internal tide generation models. Deep-Sea Research 29, 307–338.

Brandt, P., Romeiser, R., Rubino, A., 1999. On the determination of characteristics of the interior ocean dynamics from radar signatures of internal solitary waves. Journal of Geophysical Research 104, 30039–30045.

Da Silva, J.C.B., Ermakov, S.A., Robinson, I.S., Jeans, D.R.G., Kijashko, S.V., 1998. Role of surface films in ERS SAR signatures of internal waves on the shelf. 1. Short-period internal waves. Journal of Geophysical Research 103, 8009–8031.

Ermakov, S.A., Salashin, S.G., Panchencko, A.R., 1992. Film slicks on the sea surface and some mechanisms of their formation. Dynamics of Atmospheres and Oceans 16, 279–304.

Gerkema, T., 1996. A unified model for the generation and fission of internal tides in a rotating ocean. Journal of Marine Research 54, 421–450.

Gerkema, T., 2001. Internal and interfacial tides: beam scattering and local generation of solitary waves. Journal of Marine Research 59, 227–255.

Holligan, P.M., Pingree, R.D., Mardell, G.T., 1985. Oceanic solitons, nutrient pulses and phytoplankton growth. Nature 314, 348–350.

Konyaev, K.V., Sabinin, K.D., Serebryany, A.N., 1995. Large-amplitude internal waves at the Mascarene Ridge in the Indian Ocean. Deep-Sea Research Part I 42, 2075–2091.

Liu, A.K., Holbrook, J.R., Apel, J.R., 1985. Nonlinear internal wave evolution in the Sulu Sea. Journal of Physical Oceanography 15, 1613–1624.

New, A.L., 1988. Internal tidal mixing in the Bay of Biscay. Deep-Sea Research 35, 691–709.

New, A.L., Esteban, M., 1999. A new Korteweg-de Vries-type theory for internal solitary waves in a rotating continuously-stratified ocean. In: Pelinovsky, E.N., Talanov, V.I. (Eds.), Ocean Subsurface Layer: Physical Processes and Remote Sensing. Pub.s: Applied Physics Institute Press, Nizhny Novgorod, Russia. June 1999, pp. 173–203.

New, A.L., Pingree, R.D., 1990a. Large-amplitude internal soliton packets in the central Bay of Biscay. Deep-Sea Research 37, 513–524.

New, A.L., Pingree, R.D., 1990b. Evidence for internal tidal mixing near the shelf break in the Bay of Biscay. Deep-Sea Research 37, 1783–1803.

New, A.L., Pingree, R.D., 1992. Local generation of internal soliton packets in the central Bay of Biscay. Deep-Sea Research 39, 1521–1534.

New, A.L., Pingree, R.D., 2000. An intercomparison of internal solitary waves in the Bay of Biscay and resulting from Korteweg-de Vries-type theory. Progress in Oceanography 45, 1–38.

Pingree, R.D., Mardell, G.T., 1985. Solitary internal waves in the Celtic Sea. Progress in Oceanography 14, 431–441.

Pingree, R.D., Morrison, G.K., 1973. The relationship between stability and source waters for a section in the Northeast Atlantic. Journal of Physical Oceanography 3, 280–285.

Pingree, R.D., New, A.L., 1989. Downward propagation of internal tidal energy into the Bay of Biscay. Deep-Sea Research 36, 735–758.

Pingree, R.D., New, A.L., 1991. Abyssal penetration and bottom reflection of internal tidal energy in the Bay of Biscay. Journal of Physical Oceanography 21, 28–39.

Pingree, R.D., New, A.L., 1995. Structure, seasonal development and sunglint spatial coherence of the internal tide on the Celtic and Armorican shelves and in the Bay of Biscay. Deep-Sea Research Part I 42, 245–284.

Pingree, R.D., Mardell, G.T., New, A.L., 1986. Propagation of internal tides from the upper slopes of the Bay of Biscay. Nature 321, 154–158.

Serpette, A., Mazé, R., 1989. Internal tides in the Bay of Biscay: a two-dimensional model. Continental Shelf Research 9, 795–821.

Thompson, D.R., Gasparovic, R.F., 1986. Intensity modulation in SAR images of internal waves. Nature 320, 345–348.